Critical Point of Symmetric Binary Homopolymer Blends

Russell K. W. Spencer* and Mark W. Matsen*

Department of Chemical Engineering, Department of Physics & Astronomy, and Waterloo Institute for Nanotechnology, University of Waterloo, Waterloo, Ontario, Canada

E-mail: r6spenc@uwaterloo.ca; mwmatsen@uwaterloo.ca

Abstract

Monte Carlo field-theoretic simulations (MC-FTS) are performed on structurally symmetric binary homopolymer blends for invariant polymerization indexes of $\bar{N} \geq 10^3$. It is shown that the ultraviolet (UV) divergence that plagues MC-FTS at small $\bar{N}$ can be removed by an appropriate renormalization of the Flory-Huggins interaction parameter, χ, allowing one to extract meaningful results that are independent of the wavevector cutoff. Once the divergence is taken care of, the fluctuation corrections to mean-field theory are found to be exceptionally small. In particular, the disordered-state structure function, $S(k)$, is virtually indistinguishable from the RPA prediction, and there is a slight shift in the critical point, $(\chi N)_c$, that roughly scales as $\bar{N}^{-1/2}$. An implication of the small corrections is that previous experimental determinations of χ based on homopolymer blends should be relatively accurate.

*To whom correspondence should be addressed

INTRODUCTION

The theory of binary homopolymer blends developed by Flory[1] and Huggins[2] has long been a standard topic of polymer textbooks. The focus is typically on structurally symmetric blends involving polymers of the same molecular volume, $v_m = N/\rho_0$, and average end-to-end length, $R_0 = aN^{1/2}$, where ρ_0^{-1} is the segment volume, N is the number of segments in each polymer and a is the statistical segment length. For blends of 50:50 composition, the onset of macrophase separation is predicted to occur at a critical point of $(\chi N)_c = 2$, where χ is the usual Flory-Huggins interaction parameter.

The Flory-Huggins theory corresponds to the mean-field approximation of the standard incompressible Gaussian chain model, upon which most calculations in polymer theory are based.[3,4] The mean-field predictions become exact in the infinite molecular-weight limit, and the deviations for large finite polymers are believed to depend solely on the ratio $R_0^3/v_m = \bar{N}^{1/2}$, where $\bar{N} \equiv a^6\rho_0^2 N$ is referred to as the invariant polymerization index. A recent renormalized one-loop (ROL) calculation by Qin and Morse[5] predicts

$$(\chi N)_c = 2 + 3.7\bar{N}^{-1/2} \tag{1}$$

Our aim is to test this prediction with simulation.

Not surprisingly, the critical point has been examined by a number of previous simulations.[6–11] For instance, Müller[6,7] reported a critical point of $(\chi N)_c = 2.27$ for $\bar{N} = 240$, which agrees well with eq 1. Other studies[8,9] have shown that the fluctuation correction scales as $\bar{N}^{-1/2}$, although ref 9 predicted a much larger proportionality factor of about 10. The simulations, however, were all performed using different models than the standard one, and consequently a direct comparison to eq 1 is contingent on an appropriate definition of χ. The typical definition introduced by Müller and Binder[10] matches the internal energy of the simulation to that of the Flory-Huggins theory in the athermal limit, which ensures that $(\chi N)_c \to 2$ as $\bar{N} \to \infty$.[8,9] This generally leads to an effective interaction parameter,

$\chi_e = z\epsilon/k_BT$, that is proportional to the unfavorable interaction energy, ϵ, between A and B monomers and the average number of intramolecular contacts, z, a monomer experiences in the athermal limit. Müller and coworkers evaluate z at the finite polymerization N of their simulation, but this imparts χ with an unnatural N dependence. To remedy this, Qin and Morse[5] reevaluated previous results,[6,7,11] using z_∞ obtained by extrapolating z to infinite N. It turns out that the difference between using z and z_∞ is as big as the fluctuation correction itself, and furthermore the correction fails to exhibit a universal dependence on $\bar{N}$. Since then, it has been shown[12] that this *linear* definition of χ_e also fails to produce a universal correction for the order-disorder transition of diblock copolymer melts. Fortunately, the problem was resolved by allowing a nonlinear dependence on ϵ.[12,13] As of yet, however, eq 1 has not been tested with the nonlinear definition of χ_e.

Direct simulation of the standard model is impossible due to the fact it treats the blend as an incompressible melt of one-dimensional threads interacting via point-like contact forces, but it can be done indirectly by transforming to an equivalent field-based model.[14] This involves introducing auxiliary fields, so as to replace particle-particle interactions with particle-field interactions. For A+B homopolymer blends, there are two fields: a composition field, $W_-(\mathbf{r})$, that couples to the difference in A and B concentrations and a pressure field, $W_+(\mathbf{r})$, that couples to the total concentration. In the absence of direct interactions, the polymer coordinates can be integrated out resulting in a mathematically equivalent field-based Hamiltonian, $H_f[W_-, W_+]$, that depends only on the fields. The one complication, however, is that $W_+(\mathbf{r})$ is an imaginary-valued field, which implies that the Boltzmann weight, $\exp(-H_f[W_-, W_+]/k_BT)$, is no longer a positive real-valued function. Consequently, standard simulation methods cannot be applied. Fredrickson and coworkers[14–16] have dealt with this by performing complex Langevin simulations (CL-FTS). Schmid and coworkers[15,17] have proposed a different strategy whereby the integration over $W_+(\mathbf{r})$ is performed with a saddle-point approximation, which amounts to enforcing incompressibility within the mean-field approximation. Because the saddle-point, $w_+(\mathbf{r})$, is a real-valued function, the statistical

mechanics can then be performed using standard Monte Carlo simulations (MC-FTS). Although both types of FTS have been applied to binary homopolymer blends,[15–17] simulations have so far been limited to two dimensions.

Here, we extend the MC-FTS to three dimensions, but before doing so we must deal with an ultraviolet (UV) divergence. In FTS, the fields are represented on a spatial grid with some specified spacing Δ, and the simulations should, in principle, become increasingly accurate as $\Delta \to 0$. However, previous MC-FTS for diblock copolymers[18] found that melts tend to disorder as Δ is decreased due to a UV divergence. It is a weak logarithmic divergence in two dimensions, but in three dimensions the effect is proportional to the maximum wavevector allowed by the discrete grid. Fortunately, Olvera de la Cruz et al.[19] have shown that the divergence can be compensated for by an appropriate increase in the bare χ_b used in the simulations, or equivalently by expressing results in terms of an effective

$$\chi_{e1} = \left(1 - \frac{6\alpha}{\pi^2} l\Lambda\right) \chi_b \tag{2}$$

where $l = R_0 \bar{N}^{-1/2}$ is the invariant segment length. For cubic simulation boxes with a regular grid, $\Lambda = \pi/\Delta$ and $\alpha = 1.221$.[18] The renormalization works well for large $\bar{N}$, but eventually fails as the prefactor in front of χ_b approaches zero. Vorselaars and Matsen[20] derived an alternative χ_{e2} motived by the approach of Müller and Binder,[10] which appears to work to much smaller values of $\bar{N}$. Both definitions of χ_e will be tested in this study.

THEORY

This section describes our Monte Carlo field-theoretic simulation (MC-FTS) for a binary blend, where the first $n_{\rm A}$ homopolymer molecules are of type A and the remaining $n_{\rm B}$ are of type B. The total number of molecules, $n \equiv n_{\rm A} + n_{\rm B} = \bar{N}^{1/2} V/R_0^3$, is proportional to the volume, V, of the system. The MC-FTS is based on the standard incompressible Gaussian-chain model, in which the α'th *coarse-grained* molecule experiences an entropic stretching

penalty of

$$S_\alpha = -\frac{3k_B}{2R_0^2}\int_0^1 |\mathbf{r}'_\alpha|^2 ds \tag{3}$$

where its configuration, $\mathbf{r}_\alpha(s)$, is specified in terms of a parameter, s, that runs along its contour. The unlike molecules interact by simple pairwise contact forces, for which the internal energy is expressed as

$$\hat{U} = k_B T \rho_0 \chi_b \int \hat{\phi}_A(\mathbf{r})\hat{\phi}_B(\mathbf{r}) d\mathbf{r} \tag{4}$$

where

$$\hat{\phi}_A(\mathbf{r}) = \frac{N}{\rho_0}\sum_{\alpha=1}^{n_A}\int_0^1 \delta(\mathbf{r}-\mathbf{r}_\alpha) ds \tag{5}$$

is a dimensionless A concentration, and $\hat{\phi}_B(\mathbf{r})$ is a B concentration given by an analogous expression with $\alpha = n_A + 1$ to n. As such, the particle-based Hamiltonian is $H_p[\{\mathbf{r}_\alpha\}] = \hat{U} - T\sum_\alpha S_\alpha$, and the partition function for a canonical ensemble is

$$Z \sim \int \exp\left(-\frac{H_p[\{\mathbf{r}_\alpha\}]}{k_B T}\right)\delta[\hat{\phi}_A + \hat{\phi}_B - 1]\prod_{\alpha=1}^{n}\mathcal{D}\mathbf{r}_\alpha \tag{6}$$

where the delta functional enforces incompressibility. For simplicity, we ignore the factor of $(n_\mathrm{A}! n_\mathrm{B}!)^{-1}$ accounting for the indistinguishability among molecules of the same type.[4]

To proceed, we switch to a mathematically equivalent field-based model by performing standard transformations[3,4,21] that convert the partition function to

$$Z \sim \int \exp\left(-\frac{H_f[W_-, W_+]}{k_B T}\right)\mathcal{D}W_-\mathcal{D}W_+ \tag{7}$$

where the integration is now over a composition field, $W_-(\mathbf{r})$, that acts on $\hat{\phi}_-(\mathbf{r}) \equiv \hat{\phi}_A(\mathbf{r}) - \hat{\phi}_B(\mathbf{r})$ and a pressure field, $W_+(\mathbf{r})$, that acts on $\hat{\phi}_+(\mathbf{r}) \equiv \hat{\phi}_A(\mathbf{r}) + \hat{\phi}_B(\mathbf{r})$. The resulting

field-based Hamiltonian takes the form

$$\frac{H_f[W_-,W_+]}{nk_BT} = -\bar{\phi}_A \ln Q_A - \bar{\phi}_B \ln Q_B + \frac{1}{V}\int\left(\frac{W_-^2}{\chi_b N} - W_+\right)d\mathbf{r} \quad (8)$$

where $\bar{\phi}_\gamma = n_\gamma/n$ is the volume average of $\hat{\phi}_\gamma$ and

$$Q_\gamma[W_-,W_+] = \int q_\gamma(\mathbf{r},1)d\mathbf{r} \quad (9)$$

is the single-chain partition function for the γ-type homopolymer ($\gamma = A$ or B). The latter is calculated from a partial partition function, $q_\gamma(\mathbf{r},s)$, that satisfies

$$\frac{\partial q_\gamma}{\partial s} = \frac{R_0^2}{6}\nabla^2 q_\gamma - W_\gamma q_\gamma \quad (10)$$

with the initial condition $q_\gamma(\mathbf{r},0) = 1$. The field acting on A homopolymers is $W_A(\mathbf{r}) = W_+(\mathbf{r}) + W_-(\mathbf{r})$, while the one for B homopolymers is $W_B(\mathbf{r}) = W_+(\mathbf{r}) - W_-(\mathbf{r})$. Calculations for the grand-canonical ensemble just involve switching the Hamiltonian to[22]

$$\frac{H_f[W_-,W_+]}{nk_BT} = -z_A Q_A - z_B Q_B + \frac{1}{V}\int\left(\frac{W_-^2}{\chi_b N} - W_+\right)d\mathbf{r} \quad (11)$$

where $z_\gamma \equiv \exp(\mu_\gamma/k_BT)$ and μ_γ is the chemical potential of the γ-type homopolymer.

Simulation Method. To evaluate thermodynamic quantities in the field-based representation, functional integrations need to be performed over $W_-(\mathbf{r})$ and $W_+(\mathbf{r})$. They are often estimated using the saddle-point approximation, which equates to mean-field theory, but they can also be performed by simulation (i.e., FTS). As mentioned before, $W_+(\mathbf{r})$ takes on imaginary values, which precludes standard simulation techniques. However, the problem can be avoided by just simulating the fluctuations in $W_-(\mathbf{r})$ and using the saddle-point ap-

proximation for $W_+(\mathbf{r})$. This is done by setting $W_+(\mathbf{r})$ to the saddle point of the Boltzmann weight, which is the pressure field, $w_+(\mathbf{r})$, that enforces $\phi_+(\mathbf{r}) = 1$ where

$$\phi_+(\mathbf{r}) = \sum_\gamma \frac{V\bar{\phi}_\gamma}{Q_\gamma} \int_0^1 q_\gamma(\mathbf{r}, s) q_\gamma(\mathbf{r}, 1-s) ds \tag{12}$$

in canonical ensemble or

$$\phi_+(\mathbf{r}) = \sum_\gamma z_\gamma \int_0^1 q_\gamma(\mathbf{r}, s) q_\gamma(\mathbf{r}, 1-s) ds \tag{13}$$

in the grand-canonical ensemble. As it turns out, $w_+(\mathbf{r})$ is real valued, and so we can then employ standard Monte Carlo techniques.

Our MC simulations are performed for a cubic box of volume $V = L^3$ with periodic boundary conditions, in which $W_-(\mathbf{r})$ is defined on a regular grid of uniform spacing Δ. Each Monte Carlo step (MCS) involves a small random change in $W_-(\mathbf{r})$. We alternate between a real-space move, where the change in $W_-(\mathbf{r})$ at each grid point is selected from a uniform distribution, and a Fourier-move, where the change in $W_-(\mathbf{k})$ at each wavevector is selected from a uniform distribution weighted by the RPA structure function, $S_{\mathrm{RPA}}(k)$, evaluated at $\chi N = 1.8$. For the grand-canonical ensemble, a third move is included, where the whole $W_-(\mathbf{r})$ is shifted by a constant also generated from a uniform distribution. The amplitude of each move is tuned during the beginning of the equilibration period so as to achieve an acceptance rate of $\sim$40%.

The saddle point needs to be located after each change in $W_-(\mathbf{r})$, which is done by adjusting $w_+(\mathbf{r})$ iteratively using Anderson mixing,[23,24] until

$$\left[\frac{1}{V}\int (\phi_+ - 1)^2 d\mathbf{r}\right]^{1/2} < \varepsilon \tag{14}$$

where $\varepsilon = 10^{-4}$ for the canonical ensemble and $\varepsilon = 10^{-7}$ for the grand-canonical ensemble. In order to calculate $q_\gamma(\mathbf{r}, s)$, the diffusion equation is solved using a fourth-order pseudo-

spectral method,[23] which involves fast Fourier transforms to a regular grid in reciprocal space with a spacing of $\Delta k = 2\pi/L$ extending over the range $\pm\Lambda$ in each dimension, where the wavevector cutoff is $\Lambda = \pi/\Delta$. The step-size along the polymer chain, Δs, is take to be 0.05. Once $w_+(\mathbf{r})$ is known, the energy of the new configuration is evaluated using $H_f[W_-, w_+]$, and then the move is accepted or rejected using the standard Metropolis criterion.[18]

As usual, a simulation starts with a large number of MCS (e.g., 10^5) to equilibrate the system, followed by an even larger number (typically between 10^7 and 10^8) over which statistics are collected for various observables. The observables are generally sampled once every 10^2 MCS. In many cases, we are interested in collecting the statistics for an observable, $\hat{O}$, over an interval of $\chi_b N$ spanning the critical point. In order to reduce the computational effort, we employ Monte Carlo reweighting,[26,27] where m observations of $\hat{O}$ and

$$\hat{I} \equiv \frac{1}{V}\int W_-^2 d\mathbf{r} \tag{15}$$

are stored over one long simulation at a $(\chi_b N)^*$ close to the expected transition. The ensemble average of $\hat{O}$ at $\chi_b N$ is then given by

$$\langle \hat{O} \rangle = \frac{1}{m}\sum_{i=1}^{m} \hat{O}_i \exp\left(n \left[\frac{1}{(\chi_b N)^*} - \frac{1}{\chi_b N} \right] \hat{I}_i \right) \tag{16}$$

The reweighing will fail when $\chi_b N$ differs too much from $(\chi_b N)^*$, if the configurations generated at $(\chi_b N)^*$ are not sufficiently representative of those at $\chi_b N$. Fortunately, reweighting works particularly well near critical points, due to the broad distribution of configurations resulting from the critical fluctuations.

Structure Function. The first observable we consider is the disordered-state structure function

$$S(k) = \frac{\rho_0^2}{V}\langle \delta\hat{\phi}_A(\mathbf{k})\delta\hat{\phi}_A(-\mathbf{k})\rangle \tag{17}$$

where $\delta\hat{\phi}_{\rm A}(\mathbf{k})$ is the Fourier transform of $\delta\hat{\phi}_{\rm A}(\mathbf{r}) \equiv \hat{\phi}_{\rm A}(\mathbf{r}) - \bar{\phi}_{\rm A}$. It depends only on the

magnitude of the wavevector, $k \equiv |\mathbf{k}|$, and has a single peak at $k = 0$ that diverges as the critical point is approached. To evaluate $S(k)$ in FTS, the composition fluctuations in eq 17 are reexpressed in terms of fluctuations in the composition field

$$\frac{S(k)}{\rho_0 N} = \frac{n\langle W_-(\mathbf{k})W_-(-\mathbf{k})\rangle}{(V\chi_b N)^2} - \frac{1}{2\chi_b N} \tag{18}$$

as derived in the Appendix.

The random-phase approximation (RPA)[28] of the structure function is

$$\frac{S_{\rm RPA}(k)}{\rho_0 N} = \left(\frac{1}{\bar{\phi}_A\bar{\phi}_B g(\frac{1}{6}k^2R_0^2)} - 2\chi N\right)^{-1} \tag{19}$$

where $g(x) \equiv 2[\exp(-x)+x-1]/x^2$ is the Debye function. Its peak $S_{\rm RPA}(0) = \rho_0 N/(4-2\chi N)$ diverges at the mean-field critical point, and thus $S_{\rm RPA}(k)$ is regarded as the mean-field approximation of $S(k)$.

Binder Cumulant. The critical point can, in principle, be determined from the divergence in $S(0)$. However, accurate predictions would require extraordinarily large simulation boxes, because of the large-wavelength fluctuations that emerge as the critical point is approached. To obtain accurate estimates of $(\chi N)_c$ with small simulation boxes, we employ the finite-scaling method of Binder.[29] This involves calculating the fourth-order cumulant

$$U_L = 1 - \frac{\langle\bar{\phi}_-^4\rangle}{3\langle\bar{\phi}_-^2\rangle^2} \tag{20}$$

as a function of $\chi_b N$ for a series of system sizes, L, in the grand-canonical ensemble. The moments of the volume-average composition, $\bar{\phi}_-$, are given by the expressions

$$\langle\bar{\phi}_-^2\rangle = \frac{4\langle\bar{W}_-^2\rangle}{(\chi_b N)^2} - \frac{2}{n(\chi_b N)} \tag{21}$$

$$\langle\bar{\phi}_-^4\rangle = \frac{16\langle\bar{W}_-^4\rangle}{(\chi_b N)^4} - \frac{12\langle\bar{W}_-^2\rangle}{n(\chi_b N)^3} + \frac{12}{n^2(\chi_b N)^2} \tag{22}$$

derived in the Appendix. The critical point corresponds to the fixed point of U_L, or in other words the value of $\chi_b N$ for which U_L is independent of L.

Effective Interaction Parameter. To obtain meaningful results, the ultraviolet divergence needs to be removed. Its effect can be understood by looking at the internal energy, $U = \langle \hat{U} \rangle$, which can be expressed as

$$\begin{aligned} \frac{U}{k_B T \rho_0 V} &= \chi_b \bar{\phi}_A \bar{\phi}_B - \frac{\chi_b}{V} \int \langle \delta\hat{\phi}_A(\mathbf{r}) \delta\hat{\phi}_A(\mathbf{r}) \rangle d\mathbf{r} \\ &= \chi_b \bar{\phi}_A \bar{\phi}_B - \frac{\chi_b}{V(2\pi)^3} \int \langle \delta\hat{\phi}_A(\mathbf{k}) \delta\hat{\phi}_A(-\mathbf{k}) \rangle d\mathbf{k} \\ &= \chi_b \bar{\phi}_A \bar{\phi}_B \left(1 - \frac{\int S(\mathbf{k}) d\mathbf{k}}{(2\pi)^3 \rho_0^2 \bar{\phi}_A \bar{\phi}_B} \right) \end{aligned} \tag{23}$$

where we have substituted the incompressibility condition, $\hat{\phi}_{\mathrm{B}}(\mathbf{r}) = 1 - \hat{\phi}_{\mathrm{A}}(\mathbf{r})$, into eq 4 and used the definition of the structure function in eq 17. The problem is that the integral in eq 23 diverges; extending the upper limit of the integral to larger wavevectors causes a continuous decrease in U, which reduces the segregation between the A and B homopolymers.

To remove the divergence, Vorselaars and Matsen[20] took an analogous approach to the one Müller and Binder[10] used to define χ_e for particle-based simulations. That is they matched the internal energy of the MC-FTS to the Flory-Huggins expression

$$\frac{U}{k_B T \rho_0 V} = \chi_e \bar{\phi}_A \bar{\phi}_B \tag{24}$$

in the athermal limit (i.e., $\chi_e \to 0$). In this limit, the structure function in MC-FTS reduces to $S_{\mathrm{RPA}}(k)$,[20] and so it follows that the effective interaction parameter is

$$\chi_{e2} = \left(1 - l \frac{R_0^2 \int S_{\mathrm{RPA},0}(k) d\mathbf{k}}{(2\pi)^3 \rho_0 N \bar{\phi}_A \bar{\phi}_B} \right) \chi_b \tag{25}$$

where $S_{\mathrm{RPA},0}(k) = \rho_0 N \bar{\phi}_A \bar{\phi}_B g(\frac{1}{6} k^2 R_0^2)$ is the RPA structure function evaluated at $\chi N = 0$. Note that the alternative χ_{e1} in eq 2 is obtained using the large-k approximation $g(x) \approx 2/x$,

which implies that both definitions become identical as $\bar{N} \to \infty$.

RESULTS

Our study concentrates on symmetric blend compositions with $\bar{\phi}_A = \bar{\phi}_B = 1/2$ in the canonical ensemble and $z_A = z_B = 1$ in the grand-canonical ensemble. We begin by investigating the effect of the UV divergence on the structure function, $S(k)$, and testing the ability of the effective interaction parameters, χ_{e1} and χ_{e2}, to remove it. Once the divergence is dealt with, the critical point point is located using the fourth-order cumulant, U_L. Simulations are performed for invariant polymerizations extending from $\bar{N} = 10^5$, where the UV divergence is weak and fluctuation effects are negligible, down to an experimentally realistic value of $\bar{N} = 10^3$.

Structure Function. Figure 1 shows $S(k)$ calculated for different grid resolutions, Δ, using the canonical ensemble with a simulation box of size $L = 6R_0$. The first column of plots are from simulations conducted at a fixed $\chi_b N = 1.9$, for different values of $\bar{N}$. They all show a reduction in $S(k)$ as Δ decreases, which becomes more pronounced for the smaller values of $\bar{N}$. This can be attributed to the UV divergence, whereby the inclusion of shorter wavelength fluctuations permitted by the finer grids reduces the segregation of the melt. The middle column corresponds to simulations performed at a fixed value of $\chi_{e1} N = 1.9$. In this case, the divergence is nicely removed as evident by the collapse of the data, even for the lowest value of $\bar{N} = 10^3$ where the UV divergence is strongest. The final column of plots are for $\chi_{e2} N = 1.9$. Although χ_{e2} collapses the data at $\bar{N} = 10^5$, it does not perform nearly as well as χ_{e1} does at the smaller values of $\bar{N}$.

We now turn our attention to the peak of the structure function at $k = 0$, which requires us to switch to the grand-canonical ensemble. In the thermodynamic limit (i.e., $L \to \infty$), the peak diverges as $\chi N \to (\chi N)_c$ from below, and so Figure 2 plots $S^{-1}(0)$ as a function of χN, for which the RPA predicts a linear relationship. To save computational effort, the

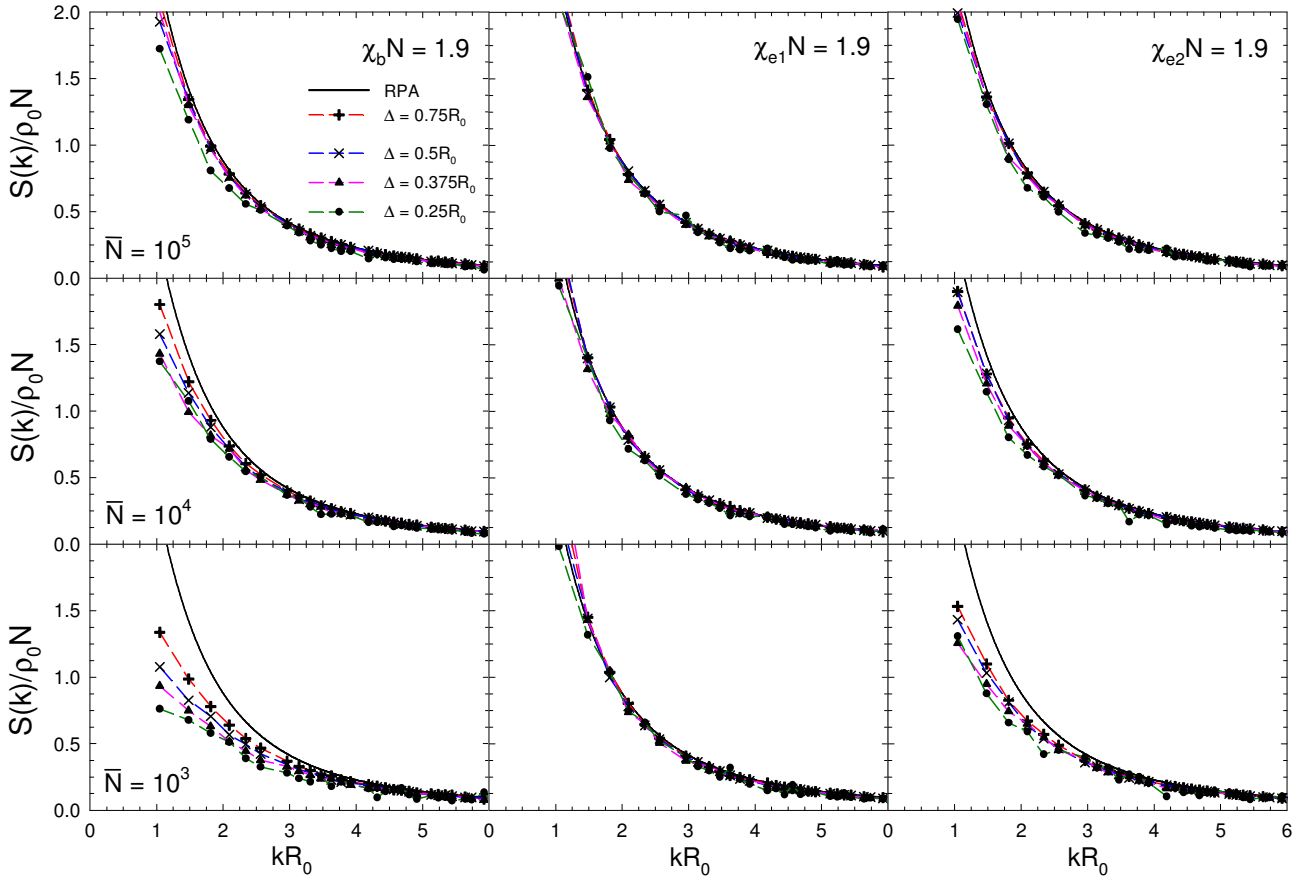


Figure 1: Structure function, $S(k)$, calculated for different grid spacings, Δ, at $\chi_b N = 1.9$ (left column), $\chi_{e1} N = 1.9$ (middle column) and $\chi_{e2} N = 1.9$ (right column) for $\bar{N} = 10^5$ (top row), $\bar{N} = 10^4$ (middle row) and $\bar{N} = 10^3$ (bottom row). The RPA prediction from eq 19 is denoted by solid black curves.

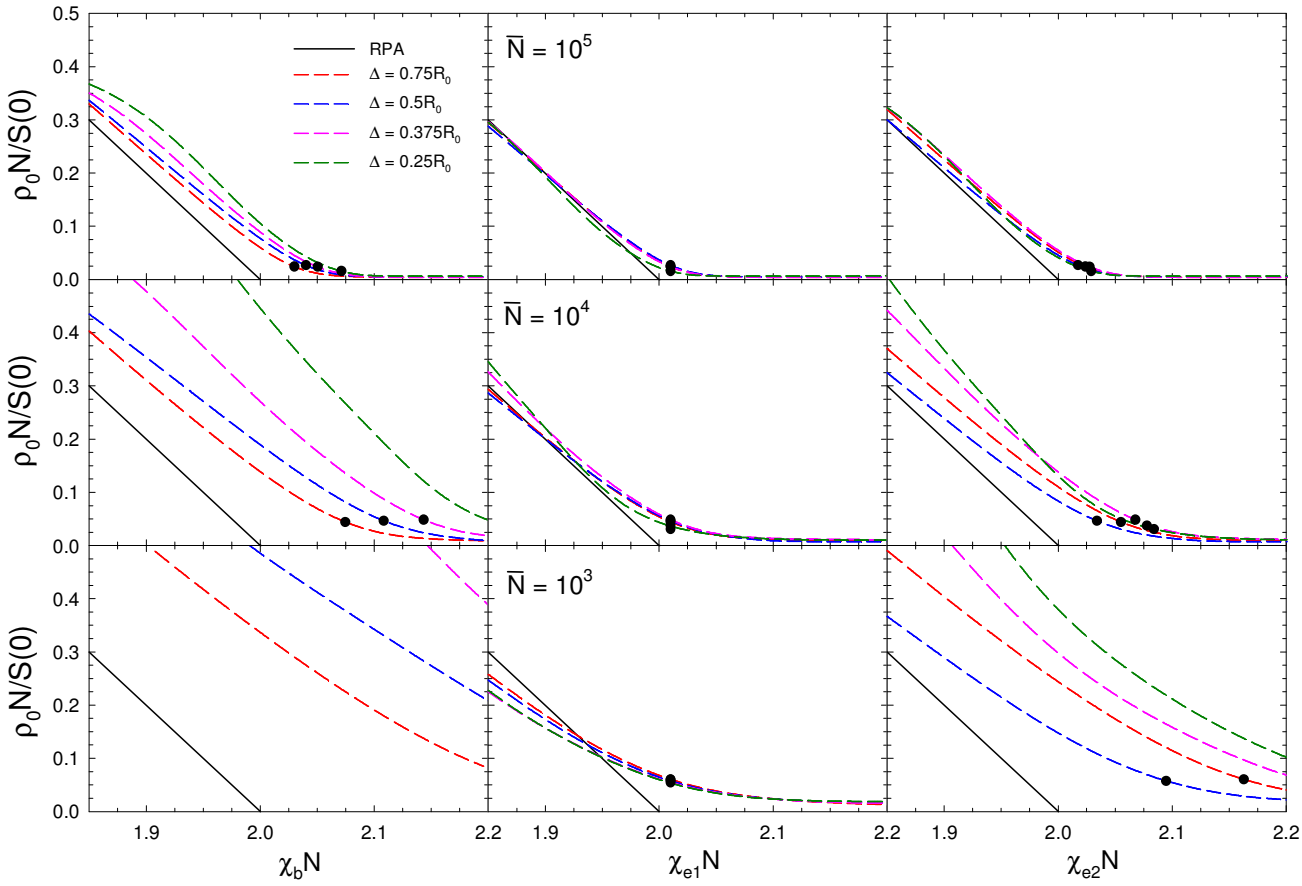


Figure 2: Inverse of the peak in the structure function, $S^{-1}(0)$, calculated using different grid spacings, Δ, and plotted as a function of $\chi_b N$ (left column), $\chi_{e1} N$ (middle column) and $\chi_{e2} N$ (right column) for $\bar{N} = 10^5$ (top row), $\bar{N} = 10^4$ (middle row) and $\bar{N} = 10^3$ (bottom row). The points about which the MC reweighting was performed are marked by solid dots, and the RPA prediction is denoted by solid black lines.

χN dependence is determined by the reweighting scheme in eq 16. The first column displays the results for different $\bar{N}$ plotted in terms of the bare χ_b. The UV divergence is even more pronounced than before. However, the curves again collapse when expressed in terms of χ_{e1} as demonstrated in the middle column. The same is not true when $S^{-1}(0)$ is plotted in terms of χ_{e2} as illustrated by the last column. In fact, the failure of χ_{e2} is quite dramatic by the time $\bar{N} = 10^3$.

Interestingly, the simple RPA prediction in eq 19 appears to be remarkably accurate. The simulation results for $k \neq 0$ in the middle column of Figure 1 are indistinguishable from the RPA prediction. There are differences between the simulations and RPA for $k = 0$ in the middle column of Figure 2, but most of that is due to the finite-size effects that tend to suppress $S(0)$ near the critical point. This will become evident once we locate the critical point, which should in principle coincide with $S^{-1}(0) \to 0$. In any case, the peak height agrees well with RPA away from the critical point for $\bar{N} = 10^5$ and 10^4. For $\bar{N} = 10^3$, however, the fluctuations cause a noticeable increase in $S(0)$ relative to RPA at $\chi_{e1}N \lesssim 1.9$. The same qualitative behavior is also predicted by ROL,[5] and so this is undoubtedly a real effect that would remain as $L \to \infty$.

Critical Point. We now locate the critical point using the fourth-order cumulant, U_L, in eq 20. This is done by performing grand-canonical simulations for a series of different system sizes, L, at a fixed interaction strength, $(\chi_b N)^*$, close to the critical point.[30] For each system size, U_L is calculated as a function of $\chi_b N$ using the reweighting scheme in eq 16. Figure 3 shows results for three values of $\bar{N}$. The curves exhibit the usual behavior,[29] where U_L transitions from 0 in the mixed region towards 2/3 in the two-phase region. Furthermore, the curves cross at common fixed point, providing a precise value for the critical point, $(\chi_b N)_c$, in terms of the bare interaction parameter.

To check the consistency of the critical behavior with the expected 3D-Ising universality class, Figure 4 scales the horizontal axes of the U_L plots with respect to $L^{1/\nu}$, where $\nu = 0.62997$ is the 3D-Ising exponent for the correlation length. The curves collapse reasonably

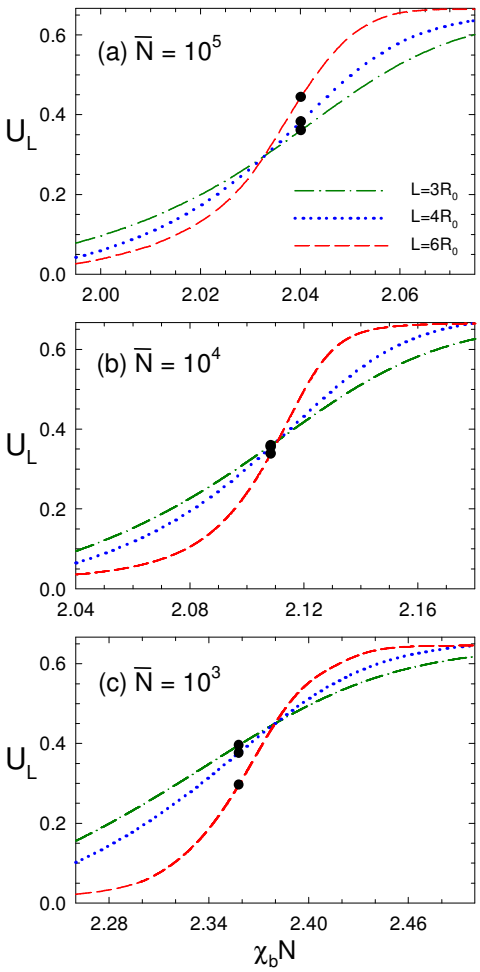


Figure 3: Fourth-order cumulant, U_L, calculated using different system sizes, L, for (a) $\bar{N} = 10^5$, (b) $\bar{N} = 10^4$ and (c) $\bar{N} = 10^3$. Simulations were conducted with a grid spacing of $\Delta = 0.5R_0$, and MC reweighting was performed about the points indicated by solid dots.

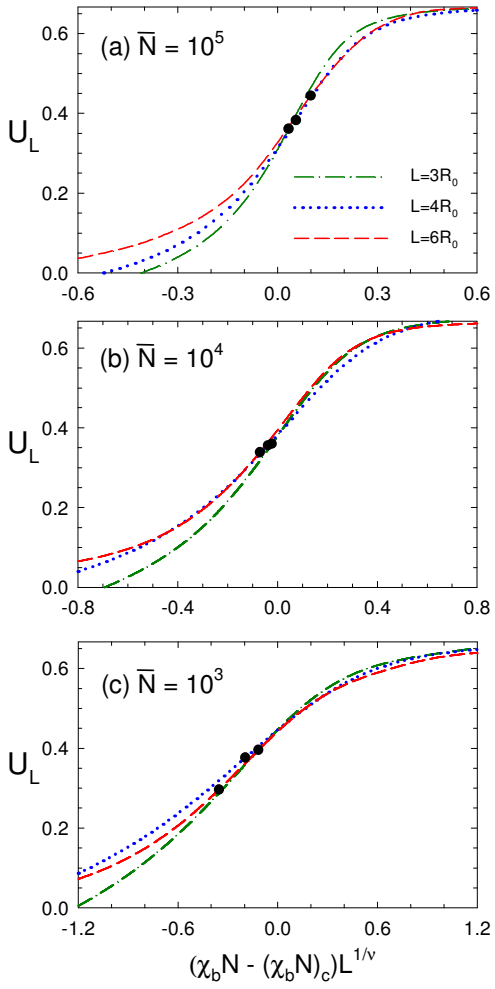


Figure 4: Analogous to Figure 3 but with the horizontal axes scaled using the 3D-Ising critical exponent, $\nu = 0.62997$.

well, particularly for the larger two system sizes. Some of the difference will be due the MC reweighing scheme, which becomes increasingly inaccurate the further $\chi_b N$ is from $(\chi_b N)^*$ denoted by the solid dots. At $\bar{N} = 10^3$, the fixed point of U_L also agrees well with the expected value, 0.47, of the 3D-Ising universality class.[25] For the higher values of $\bar{N}$, however, the fixed point drops below 0.47, which was also the case for the particle-based simulations of Müller and Binder.[10] They attributed this to the narrowing of the critical region with increasing $\bar{N}$.[11] The implication is that the system sizes need to be larger in order to observe accurate critical behavior, but unfortunately it is impractical for us to perform statistically accurate simulations for significantly larger L. Nevertheless, our main interest is in the position of the critical point, and our current simulations should be reasonably accurate in that regard, given the steepness of the U_L curves.

Table 1: Critical points, $(\chi_b N)_c$, in terms of the bare χ_b, calculated using different grid spacings, Δ, and invariant polymerization indexes, $\bar{N}$.

Δ/R_0	$(\chi_b N)_c$		
	$\bar{N} = 10^5$	$\bar{N} = 10^4$	$\bar{N} = 10^3$
0.75	2.023	2.077	2.246
0.5	2.034	2.110	2.377
0.375	2.046	2.146	2.525
0.25	2.068	2.223	2.876
0.1875	2.089	2.301	3.352

The simulations of Figure 3 were all performed for a common grid resolution of $\Delta = 0.5R_0$. In order to examine the effect of the UV divergence, the simulations are repeated for a series of different grid resolutions. The resulting positions of the critical point are tabulated in Table 1. As expected, the critical point shifts to higher $\chi_b N$ for finer grid resolutions, because the introduction of shorter wavelengths reduces the segregation between the A and B components. To remove the divergence, Figure 5 plots the critical point in terms of the effective interaction parameters, χ_{e1} and χ_{e2}, as a function of the wavevector cutoff, $\Lambda = \pi/\Delta$. In terms of χ_{e1}, the critical point approaches a constant value at large Λ, indicating that the UV divergence is removed by this renormalization of the interaction parameter. The

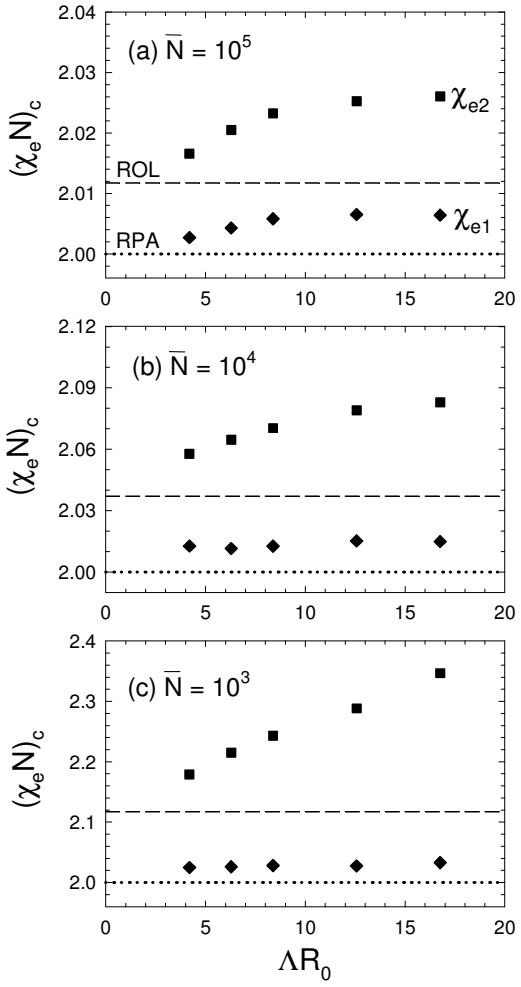


Figure 5: Critical point, $(\chi_e N)_c$, in terms of the effective χ_e in eq 2 (diamonds) and eq 25 (squares) as a function of the wavevector cutoff, $\Lambda = \pi/\Delta$, calculated for (a) $\bar{N} = 10^5$, (b) $\bar{N} = 10^4$ and (c) $\bar{N} = 10^3$. The mean-field prediction of 2 and the ROL prediction in eq 1 are denoted by the dotted and dashed lines, respectively.

alternative χ_{e2}, once again, reduces the effect of the divergence but does not completely remove it.

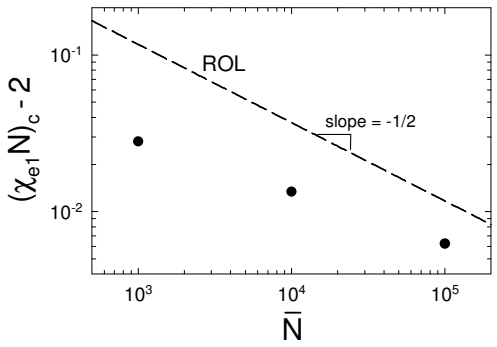


Figure 6: Logarithmic plot showing the fluctuation correction to the mean-field critical point for the three values of $\bar{N}$ simulated in this study. The dashed line denotes the ROL prediction from eq 1.[5]

For all three values of $\bar{N}$, the asymptotic value of $(\chi_{e1}N)_c$ at large Λ lies between the mean-field value of 2 and the ROL prediction in eq 1, denoted in Figure 5 by the dotted and dashed horizontal lines, respectively. This implies that the critical point approaches the mean-field value in the limit of $\bar{N} \to \infty$. Figure 6 compares the fluctuation correction, $(\chi_{e1}N)_c - 2$, from our simulations (symbols) with the ROL prediction (dashed line) on a logarithmic scale. The correction is reasonably consistent with the $\bar{N}^{-1/2}$ scaling predicted by ROL, particularly for our two largest values of $\bar{N}$. However, the proportionality factor is roughly half the predicted size, further emphasizing that fluctuation effects are extremely small in binary homopolymer blends.

DISCUSSION

Field-theoretic simulations (FTS) provide a complimentary approach to the usual particle-based simulations. To increase the $\bar{N}$ of a particle-based model requires more monomers per polymer as well as more polymers per volume R_0^3, and the extra degrees of freedom increase the computational cost of the simulation. However, this is not the case for FTS,

since the polymer degrees of freedom are integrated out of the system. Instead, FTS are only slowed down by the level of fluctuations in the fields, and consequently they are fast at large $\bar{N}$ becoming increasingly computational for small $\bar{N}$. As we have seen, the reduction in $\bar{N}$ is also accompanied by a strong UV divergence. Fortunately, the divergence can be compensated for by the simple renormalization χ_{e1} defined in eq 2, allowing for meaningful quantitative predictions of the structure function, $S(k)$, and the critical point, $(\chi N)_c$.

Despite the slight deviations from the expected 3D-Ising critical behavior, our MC-FTS estimate of $(\chi N)_c$ should be more accurate than the ROL prediction in eq 1. The ROL is a perturbative expansion truncated at first order, but more importantly it does not properly treat critical fluctuations. Although it is somewhat uncertain how well χ_{e1} removes the UV divergence from the MC-FTS, it is the same renormalization used in the ROL calculation.[5] Of course, there will be some inaccuracy in our results due to the saddle-point (i.e., mean-field) approximation for the pressure field. Nevertheless, the fluctuations of $W_-(\mathbf{r})$ are undoubtedly far more important than those of $W_+(\mathbf{r})$, and thus the MC-FTS should capture most of the deviation from mean-field theory.

The obvious way to correct for the saddle-point approximation is to use the full CL-FTS. This has already been done in two dimensions, where the CL-FTS and MC-FTS produced consistent results.[15] It would be interesting to repeat the comparison in three dimensions, but there would be a couple obstacles to deal with first. The trajectories of CL-FTS are prone to instabilities particularly when $\bar{N}$ is reduced to realistic values.[31] In fact, there is no proof that the trajectories produce stable distributions as there is for conventional Langevin simulations.[14] Furthermore, the nature of the UV divergence will change. At the very least, a as well as χ will have to be renormalized,[5] and it may be that there is no simple renormalization capable of removing the divergence for CL-FTS.

For MC-FTS, the χ_{e1} renormalization appears to work much better than it did for the diblock copolymer melts, where it started to fail when $\bar{N} \lesssim 10^4$.[20] Here, χ_{e1} works perfectly fine for values of $\bar{N}$ down to at least 10^3, perhaps because the transition occurs at a smaller

value of $\chi_{e1}N$ and because homopolymer blends do not need as fine of a spatial grid as diblock copolymer melts where the domain size is comparable to R_0. In any case, χ_{e1} will eventually fail for small $\bar{N}$, and it will be necessary to use an improved definition. Evidently, the χ_{e2} suggested by ref 20 will not do, but perhaps their other suggestions might, such as applying the procedure in ref 12 to MC-FTS or by examining higher-order corrections to the loop-expansion.

One benefit of FTS, as implemented here, is that they are based on the same standard Gaussian-chain model that underlies most theoretical calculations, which is why we can directly compare to the ROL prediction in eq 1. The standard model is generally the preferred choice because it represents the minimal model with the least number of parameters needed to represent high molecular-weight polymers. The behavior of more detailed models or in fact real experimental systems, involving for example polymers with finite persistence lengths and finite-range interactions, reduces to the mean-field behavior of the standard model in the limit of infinitely long molecules. Furthermore, it is hypothesized that the fluctuation corrections of the more complicated models will also match those of the standard model for large finite values of $\bar{N}$. To realize this universality, however, the parameters of a given model have to be properly mapped onto those of the standard model (e.g., χ and a).

In light of recent evidence[5,12] that the *linear* definition of χ_e proposed by ref 10 does not reveal the universal behavior, we cannot yet compare the previous particle-based simulations[6,7,9,10] to our MC-FTS or the ROL predictions. However, the nonlinear definition of χ_e proposed in ref 12 could permit a meaningful comparison, given its impressive performance for diblock copolymer melts.[12,13] It would just be a matter of recalibrating χ_e by applying the various models to symmetric diblock copolymer melts. Alternatively, one could study the homopolymer blends with the same models calibrated in ref 12. Either way, it will be very interesting to see if the different particle-based simulations produce consistent universal results, and furthermore if they match our MC-FTS predictions.

Determining the effective χ_e for experiments has also been an ongoing challenge. It is

generally obtained by fitting the measured structure function or phase transition of either symmetric diblock copolymer melts or symmetric homopolymer blends to theoretical predictions. The problem, however, is a lack of consistency among the different choices.[32] It is not surprising that the fits involving diblock copolymers do not produce consistent predictions for χ_e, since the mean-field[33] and fluctuation[34] theories do not provide accurate predictions for the relevant quantities. However, given recent developments, diblocks could now provide a viable system for extracting accurate values of χ_e.[35] Nevertheless, considering how small the fluctuation corrections appear to be for homopolymer blends, the previous determinations of χ_e based on homopolymer blends are probably already fairly accurate, at least for high-$\bar{N}$ systems.

SUMMARY

We have performed the first field-theoretic simulations (FTS) for binary homopolymer blends in three dimensions. The focus was on symmetric blends with equal amounts of A and B homopolymer, where both molecules contain the same number of segments, N, and both segments have the same statistical length, a (segments are defined based on a common volume of ρ_0^{-1}). The FTS employed the standard incompressible Gaussian-chain model, where polymers are treated as thin elastic threads and unlike segments interact by a simple contact force controlled by the usual Flory-Huggins interaction parameter, χ. The only approximation in the simulations was a mean-field treatment of the incompressibility condition, but this is believed to be relatively accurate. Although the FTS were strongly affected by an ultraviolet divergence, its effect was well controlled by the effective interaction parameter χ_{e1} in eq 2 originally derived by ref 19, but not by the alternative χ_{e2} in eq 25 proposed by ref 20.

The fluctuation effects were found to be exceptionally small for the range of invariant polymerization indexes examined in our study, $\bar{N} = 10^3$ to 10^5. In the disordered phase at

$\chi_{e1}N = 1.9$, the structure function, $S(k)$, was virtually indistinguishable from the mean-field prediction for $k > 0$. However, at our smallest $\bar{N}$, there was a noticeable enhancement of the peak, $S(0)$, which is qualitatively consistent with renormalized one-loop (ROL) predictions.[5] Although we observed a significant depression in the peak height at higher segregations, most of that can be attributed to finite-size effects, which become particularly pronounced near the critical point. To deal with the finite-size effects, we switched to a four-order cumulant method to locate the critical point, $(\chi N)_c$. As expected, fluctuations push the mean-field prediction, $(\chi N)_c = 2$, to higher values of χN. The shift is consistent with the $\bar{N}^{-1/2}$ scaling predicted by ROL[5] in eq 1 and earlier particle-based simulations.[8,9] However, the amplitude of the fluctuation correction is considerably smaller than previously reported. In light of how small the fluctuation effects are, the experimental practice[32] of estimating χ based on the mean-field predictions of binary homopolymer blends appears to be well justified.

Acknowledgments: We are grateful for valuable discussions with Dave Morse. This work was funded by NSF under the Center for Sustainable Polymers (CHE-1413862), and computer resources were provided by SHARCNET of Compute Canada.

APPENDIX

Here we calculate moments of the composition, $\hat{\phi}_-(\mathbf{r})$, following the approach used in ref 21. This involves adding an external potential, $U(\mathbf{r})$, to the Hamiltonian,

$$\frac{\tilde{H}_p[\{\mathbf{r}_\alpha\}]}{k_BT} = \frac{H_p[\{\mathbf{r}_\alpha\}]}{k_BT} + \frac{\rho_0}{N}\int U\hat{\phi}_- d\mathbf{r} \tag{26}$$

and evaluating the corresponding partition function, $\tilde{Z}$. With that, it immediately follows that the k'th moment is given by

$$\left\langle \prod_{i=1}^{k} \hat{\phi}_-(\mathbf{r}_i) \right\rangle = \left(-\frac{N}{\rho_0}\right)^k \frac{1}{\tilde{Z}} \left. \frac{\mathcal{D}^k \tilde{Z}}{\prod_{i=1}^{k} \mathcal{D}U(\mathbf{r}_i)} \right|_{U=0} \tag{27}$$

Performing the transformation from the particle- to field-based Hamiltonian, we obtain

$$\begin{aligned}\frac{\tilde{H}_f[W_+,W_-]}{nk_BT} &= \frac{H_f[W_+,W_-]}{nk_BT} + \\ &\frac{1}{\chi_b NV}\int(2UW_- + U^2)d\mathbf{r} \end{aligned} \tag{28}$$

A single differentiation of $\tilde{Z}$ gives the first moment

$$\begin{aligned}\langle\hat{\phi}_-(\mathbf{r})\rangle &= -\frac{2\langle W_-(\mathbf{r})+U(\mathbf{r})\rangle}{\chi_b N}\Big|_{U=0} \\ &= -\frac{2\langle W_-(\mathbf{r})\rangle}{\chi_b N}\end{aligned} \tag{29}$$

Similarly, the second moment is given by

$$\begin{aligned}\langle\hat{\phi}_-(\mathbf{r}_1)\hat{\phi}_-(\mathbf{r}_2)\rangle &= \frac{4\langle W_-(\mathbf{r}_1)W_-(\mathbf{r}_2)\rangle}{(\chi_b N)^2} - \\ &\left(\frac{N}{\rho_0}\right)\frac{2\delta(\mathbf{r}_1-\mathbf{r}_2)}{\chi_b N}\end{aligned} \tag{30}$$

Fourier transforming this expression and using the fact that $\delta\hat{\phi}_{\rm A} = \frac{1}{2}\hat{\phi}_-$ gives the field-based expression for $S(k)$ in eq 18. Integrating the expression over $\mathbf{r}_1$ and $\mathbf{r}_2$ leads directly to eq 21 for $\langle\bar{\phi}_-^2\rangle$. Lastly, the fourth moment is

$$\begin{aligned}\left\langle\prod_{i=1}^{4}\hat{\phi}_-(\mathbf{r}_i)\right\rangle &= \frac{16\langle\prod_{i=1}^{4}W_-(\mathbf{r}_i)\rangle}{(\chi_b N)^4} - \left(\frac{N}{\rho_0}\right)\frac{8\mathcal{A}}{(\chi_b N)^3} + \\ &\left(\frac{N}{\rho_0}\right)^2\frac{4\mathcal{B}}{(\chi_b N)^2}\end{aligned} \tag{31}$$

where

$$\begin{aligned}\mathcal{A} &= \langle W_-(\mathbf{r}_3)W_-(\mathbf{r}_4)\rangle\delta(\mathbf{r}_1-\mathbf{r}_2)+\\ &\quad \langle W_-(\mathbf{r}_2)W_-(\mathbf{r}_4)\rangle\delta(\mathbf{r}_1-\mathbf{r}_3)+\\ &\quad \langle W_-(\mathbf{r}_2)W_-(\mathbf{r}_3)\rangle\delta(\mathbf{r}_1-\mathbf{r}_4)+\\ &\quad \langle W_-(\mathbf{r}_1)W_-(\mathbf{r}_4)\rangle\delta(\mathbf{r}_2-\mathbf{r}_3)+\\ &\quad \langle W_-(\mathbf{r}_1)W_-(\mathbf{r}_3)\rangle\delta(\mathbf{r}_2-\mathbf{r}_4)+\\ &\quad \langle W_-(\mathbf{r}_1)W_-(\mathbf{r}_2)\rangle\delta(\mathbf{r}_3-\mathbf{r}_4) \qquad (32)\end{aligned}$$

and

$$\begin{aligned}\mathcal{B} &= \delta(\mathbf{r}_1-\mathbf{r}_2)\delta(\mathbf{r}_3-\mathbf{r}_4)+\\ &\quad \delta(\mathbf{r}_1-\mathbf{r}_3)\delta(\mathbf{r}_2-\mathbf{r}_4)+\\ &\quad \delta(\mathbf{r}_1-\mathbf{r}_4)\delta(\mathbf{r}_2-\mathbf{r}_3) \qquad (33)\end{aligned}$$

Integrating eq 31 over the four coordinates, $\mathbf{r}_1$ to $\mathbf{r}_4$, gives eq 22 for $\langle\bar{\phi}_-^4\rangle$.

References

(1) Flory, P. J. *J. Chem. Phys.* **1942**, *10*, 51–61.

(2) Huggins, M. L. *J. Phys. Chem.* **1942**, *46*, 151–158.

(3) Fredrickson, G. H. *The Equilibrium Theory of Inhomogeneous Polymers*; Oxford University Press: New York, 2006.

(4) Matsen, M. W. In *Soft Matter: Polymer Melts and Mixtures*; Gompper, G., Schick, M., Eds.; Wiley-VCH: Weinheim, Germany, 2006.

(5) Qin, J.; Morse, D. C. *J. Chem. Phys.* **2009**, *130*, 224902.

(6) Müller, M. In *Soft Matter: Polymer Melts and Mixtures*; Gompper, G., Schick, M., Eds.; Wiley-VCH: Weinheim, Germany, 2006.

(7) Müller, M.; de Pablo, J. J. *Lect. Notes Phys.* **2006**, *703*, 76–126.

(8) Müller, M. *Macromolecules* **1998**, *31*, 9044–9057.

(9) Detcheverry, F. A.; Pike, D. Q.; Nealey, P. F.; Müller, M.; de Pablo, J. J. *Phys. Rev. Lett.* **2009**, *102*, 197801.

(10) Müller, M.; Binder, B. *Macromolecules* **1995**, *28*, 1825–1834.

(11) Deutsch, H. P.; Binder, K. *J. Phys. II France* **1993**, *3*, 1049–1073.

(12) Glaser, J.; Medapuram, P.; Beardsley, T. M.; Matsen, M. W.; Morse, D. C. *Phys. Rev. Lett.* **2014**, *113*, 068302.

(13) Medapuram, P.; Glaser, J.; Morse, D. C. *Macromolecules* **2015**, *48*, 819–839.

(14) Fredrickson, G. H.; Ganesan, V.; Drolet, F. *Macromolecules* **2002**, *35*, 16–39.

(15) Düchs, D.; Ganesan, V.; Fredrickson, G. H.; Schmid, F. *Macromolecules* **2003**, *36*, 9237–9248.

(16) Riggleman, R. A.; Fredrickson, G. H *J. Chem. Phys.* **2010**, *132*, 024104.

(17) Düchs, D.; Schmid, F. *J. Chem. Phys.* **2004**, *121*, 2798–2805.

(18) Stasiak, P.; Matsen, M. W. *Macromolecules* **2013**, *46*, 8037–8045.

(19) Olvera de la Cruz, M.; Edwards, S. F.; Sanchez, I. C. *J. Chem. Phys.* **1988**, *89*, 1704–1708.

(20) Vorselaars, B.; Stasiak, P.; Matsen, M. W. *Macromolecules* **2015**, *48*, 9071–9080.

(21) Müller, M.; Schmid, F. In *Advanced Computer Simulation Approaches for Soft Matter Sciences II*; Holm, C., Binder, K., Eds.; Springer-Verlag: Berlin, Germany, 2005.

(22) Matsen, M. W. *Phys. Rev. Lett.* **1995**, *74*, 5765–5768.

(23) Stasiak, P.; Matsen, M. W. *Eur. Phys. J. E* **2011**, *34*, 110.

(24) The algorithm is the same as in ref 23 but with $d_j^{(k)} = \phi_{+,j}^{(k)} - 1$, where $\phi_{+,j}^{(k)}$ is the value of $\phi_+(\mathbf{r})$ at the j'th grid point of the k'th iteration.

(25) Ferrenberg, A. M.; Landau, D. P. *Phys. Rev. B* **1991**, *61*, 5081–5091.

(26) Ferrenberg, A. M.; Swendsen, R. H. *Phys. Rev. Lett.* **1988**, *61*, 2635–2638.

(27) Ferrenberg, A. M.; Swendsen, R. H. *Phys. Rev. Lett.* **1989**, *63*, 1195–1198.

(28) de Gennes, P. G. *Scaling Concepts in Polymer Physics*; Cornell University Press: New York, 1979.

(29) Binder, K. *Phys. Rev. Lett.* **1981**, *47*, 693–696.

(30) MC reweighting was performed at an interaction strength corresponding to $\chi_{e1}N = 2.01$.

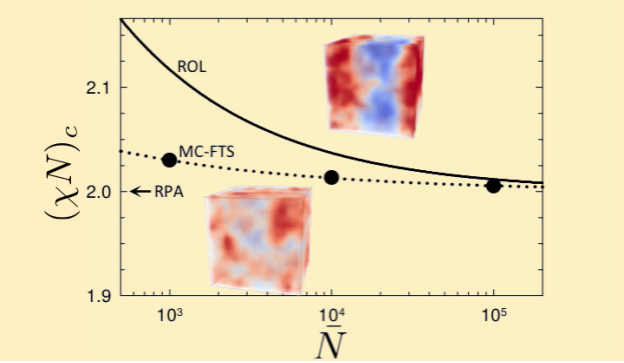
(31) Koski, J.; Chao, H.; Riggleman, R. A. J. *J. Chem. Phys.* **2013**, *139*, 244911.

(32) Maurer, W. W.; Bates, F. S; Lodge, T. P.; Almdal, K.; Mortensen, K.; Fredrickson, G. H. *J. Chem. Phys.* **1998**, *108*, 2989–3000.

(33) Leibler, L. *Macromolecules* **1980**, *13*, 1602–1617.

(34) Fredrickson, G. H.; Helfand, E. *J. Chem. Phys.* **1987**, *87*, 697–705.

(35) Gillard, T. M.; Medapuram, P.; Morse, D. C.; Bates, F. S. *Macromolecules* **2015**, *48*, 2801–2811.



for Table of Contents use only

Title: Critical Point of Symmetric Binary Homopolymer Blends

Authors: R. K. W. Spencer and M. W. Matsen